RESEARCH ARTICLE

Methods in Ecology and Evolution BRITISH ECOLOGICAL SOCIETY

BITS: A Bayesian Isotope Turnover and Sampling model for strontium isotopes in proboscideans and its potential utility in movement ecology

Deming Yang[1,2] | Gabriel J. Bowen[1] | Kevin T. Uno[1,3] | Katya Podkovyroff[1,4] |
Nancy A. Carpenter[5] | Diego P. Fernandez[1] | Thure E. Cerling[1,4]

[1]Department of Geology and Geophysics, University of Utah, Salt Lake City, Utah, USA

[2]Division of Anthropology, American Museum of Natural History, New York City, New York, USA

[3]Division of Biology and Paleo Environment, Lamont-Doherty Earth Observatory of Columbia University, Palisades, New York, USA

[4]School of Biological Sciences, University of Utah, Salt Lake City, Utah, USA

[5]Utah's Hogle Zoo, Salt Lake City, Utah, USA

Correspondence
Deming Yang
Email: deming.yang@utah.edu

Present address
Kevin T. Uno, Department of Human Evolutionary Biology, Harvard University, Cambridge, Massachusetts, USA

Abstract

1. Strontium isotope ratios ($^{87}Sr/^{86}Sr$) of incrementally grown tissues have been widely used to study movement ecology and migration of animals. However, the time scale of $^{87}Sr/^{86}Sr$ incorporation from the environment into tissue and how it may influence data interpretation are still poorly understood. Using the relocation of a zoo elephant (*Loxodonta africana*) named Misha, we characterise and model the $^{87}Sr/^{86}Sr$ turnover process using high-resolution measurements of its tusk dentine. We seek to develop a framework that can improve quantitative interpretation of $^{87}Sr/^{86}Sr$ data in tissues.

2. The $^{87}Sr/^{86}Sr$ transition associated with the relocation is measured using laser ablation inductively coupled plasma mass spectrometry (LA-ICP-MS) on a prepared tusk slab. We develop a turnover model (BITS), with a rapidly exchanging central pool and a slowly exchanging peripheral pool, in a Bayesian statistical framework. The measured dentine data are first used to calibrate model parameters. The parameters are then used to estimate possible $^{87}Sr/^{86}Sr$ input time series from two datasets via model inversion: a fidelity test using Misha's dentine data and a case study using published dentine measurements from an Alaskan Woolly Mammoth (*Mammuthus primigenius*).

3. The LA-ICP-MS data are consistent with a two-compartment turnover process with equivalent half-lives of 41 days for the central pool and 170 days for the peripheral pool. The model inversion shows good fidelity when estimating the intake $^{87}Sr/^{86}Sr$ time series associated with Misha's relocation. In the case study, the model suggests an abrupt pattern of change in, and a much wider range of, intake $^{87}Sr/^{86}Sr$ values than expressed in the woolly mammoth dentine data themselves.

4. Our framework bridges the gap between environmental $^{87}Sr/^{86}Sr$ variation and data measured in tusk dentine or other incrementally grown tissues. It could be coupled with movement models and additional isotope tracers to study seasonal

Nancy A. Carpenter—Retired.

residency or the spatial and temporal patterns of movement/migration. The generic turnover processes can be adapted to other isotope systems, additional incremental tissues, or other organisms, thus expanding our modelling toolkit to investigate niche partitioning, life history traits and behavioural patterns in conservation biology, archaeology and paleoecology.

1 | INTRODUCTION

Stable isotopes in incrementally grown tissues (e.g. hair, feathers, otoliths, dental enamel and dentine) have been used to provide temporally resolved interpretations of diet, trophic relationships and movement patterns of animals. The pathways by which an isotope tracer is incorporated into tissue have been of particular interest for ecologists (reviewed by e.g. Carter et al., 2019; Phillips & Eldridge, 2006; Vander Zanden et al., 2015) because they determine the time scale of the ecological/behavioural inferences that can be made from isotopic data (Martínez del Rio et al., 2009). Within a specific isotope system (e.g. carbon, nitrogen, oxygen or strontium), different tissues are known to exhibit different response patterns to a given intake signal (e.g. Dalerum & Angerbjörn, 2005; Hobson, 1999). While studying tissue turnover can be challenging and require controlled experiments (e.g. Gannes et al., 1997; Martínez del Rio et al., 2009; Wolf et al., 2009), models based on such studies can improve interpretations of measured isotope variation in specific tissues/organisms (e.g. Magozzi et al., 2019; Thomas & Crowther, 2015).

The utility of strontium isotope ratio data ($^{87}Sr/^{86}Sr$) in provenance and mobility studies has gained increasing attention in the recent decade (reviewed by e.g. Britton et al., 2020; Coelho et al., 2017; Crowley et al., 2017; Holt et al., 2021; Makarewicz & Sealy, 2015). High resolution and low-cost analytical methods such as laser ablation inductively coupled plasma mass spectrometry (LA-ICP-MS) and geostatistical methods (Isoscapes in e.g. Bataille et al., 2020; Bowen & West, 2008; Wunder, 2010) have facilitated data growth and geospatially explicit reconstructions of movement or migration (e.g. Brennan et al., 2015; Kowalik et al., 2023; Lazzerini et al., 2021; Willmes et al., 2016; Wooller et al., 2021). However, the pathways and timescales of $^{87}Sr/^{86}Sr$ incorporation from the environment (e.g. from food and water) to commonly studied tissues are still poorly understood. An implicit assumption of instantaneous incorporation has often been made (Wooller et al., 2021), which is most likely invalid in large-bodied animals such as proboscideans. Therefore, understanding $^{87}Sr/^{86}Sr$ turnover and accounting for its associated signal attenuation could refine the use of these data for studies of movement ecology in a geospatial context.

In this study, we investigate the process of $^{87}Sr/^{86}Sr$ incorporation into proboscidean tusk dentine using a zoo elephant that was moved between two distinct $^{87}Sr/^{86}Sr$ environments. We first document the record of $^{87}Sr/^{86}Sr$ turnover using high-resolution measurements of tusk dentine. Building on previous studies of calcium metabolism, we then develop a Bayesian Isotope Turnover and Sampling (BITS) framework that simulates the processes of $^{87}Sr/^{86}Sr$ incorporation and turnover in the animal, and its output into dentine. We demonstrate the utility of the model framework using two inverse applications to $^{87}Sr/^{86}Sr$ data from dentine and discuss its potential application to other incremental tissues and geospatial-explicit studies of movement/migration ecology. We provide context for the BITS framework by comparing it with previously published approaches.

2 | METHODS

2.1 | Experimental background and data

$^{87}Sr/^{86}Sr$ data come from tusk dentine of Misha, a female African savanna elephant (*Loxodonta africana*). Misha had been in captivity in Vallejo, CA, for about 20 years before she was relocated to Utah's Hogle Zoo in Salt Lake City, on 22 April 2005. After ca. 3.5 years of residence in UT, she was euthanized on 9 September 2008, due to rapidly declining health (Uno, Fisher, Wittemyer, et al., 2020). The Hogle Zoo agreed to loan one tusk to the University of Utah for research. The tusk was longitudinally and transversely sectioned, and a transverse slab (M640b) was prepared into a thin section for subsequent analyses (Figure 1; Data S1).

On the M640b slab (Figure 1b), mass ratios for a suite of metals including ^{87}Sr and ^{86}Sr were measured by LA-ICP-MS (detailed methods in Data S1) along a straight line perpendicular to the primary growth rings starting from the outer part of the slab toward the pulp cavity (Figure 1b). Misha's mean tusk dentine growth rate was calculated using the distance between the onset of $^{87}Sr/^{86}Sr$ increase along the laser transect, marking the date of Misha's move to Utah, and the pulp cavity surface reflecting the date of death. To document strontium sources (food, water, etc.) after Misha's relocation, we measured Sr concentration and $^{87}Sr/^{86}Sr$ of elephant feed samples from the Hogle Zoo and potential water sources using the solution method (preparation and analysis methods in Data S1). To make sure that $^{87}Sr/^{86}Sr$ data generated by the laser ablation and the solution methods are comparable, a micromill series was made on the longitudinal section of the tusk proximal to the M640b slab

FIGURE 1 (a) Schematic of Misha's tusk (dentine) and its preparation (Data S1). Figure modified from Fisher and Fox (2007) with permission. (b) Flatbed scan of the thin section (M640b) made on the transverse section toward the proximal one-third of Misha's tusk, showing the laser ablation transect and the approximate location where the move was recorded; (c) Measured $^{87}Sr/^{86}Sr$ (50-point average, y-axis) of the tusk dentine by laser ablation inductively coupled plasma mass spectrometry (LA-ICP-MS) and its associated distance (micron) from the pulp cavity (x-axis). The pulp cavity is the appositional surface for new dentine and marks Misha's date of death.
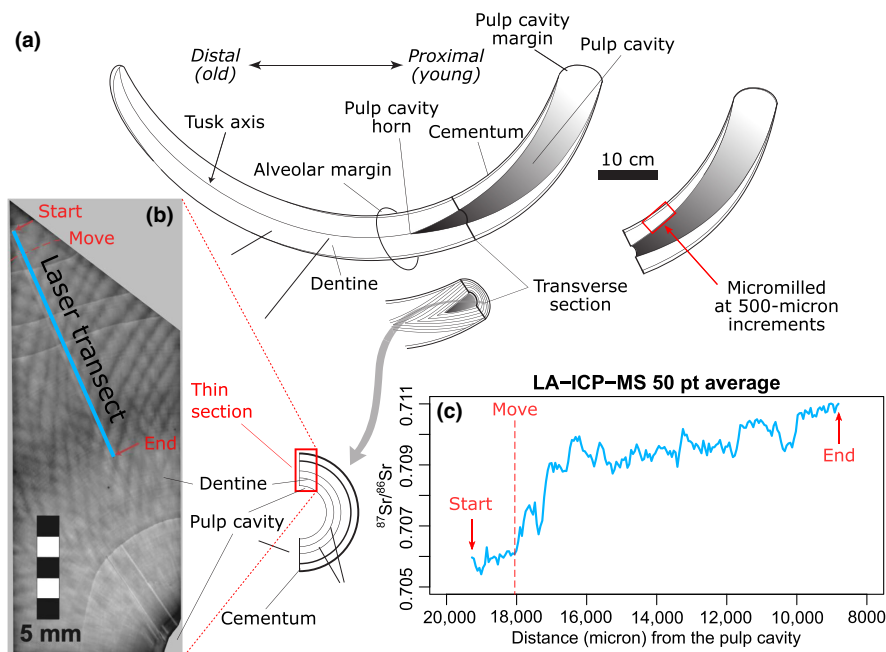

FIGURE 2 (a) Illustrations of the pools (circles) and associated mass fluxes (arrows) proposed in the Sr turnover model. Sr exchange with the immense bone pool (dashed circle) is limited to the chemically active subset that is included in Pool II (Meiggs, 2007). (b) An example of model inversion that can be used to estimate possible intake $^{87}Sr/^{86}Sr$ time series based on measured series in tusk dentine. Silhouette images from https://www.phylopic.org/, CC-BY-NC-SA 3.0.
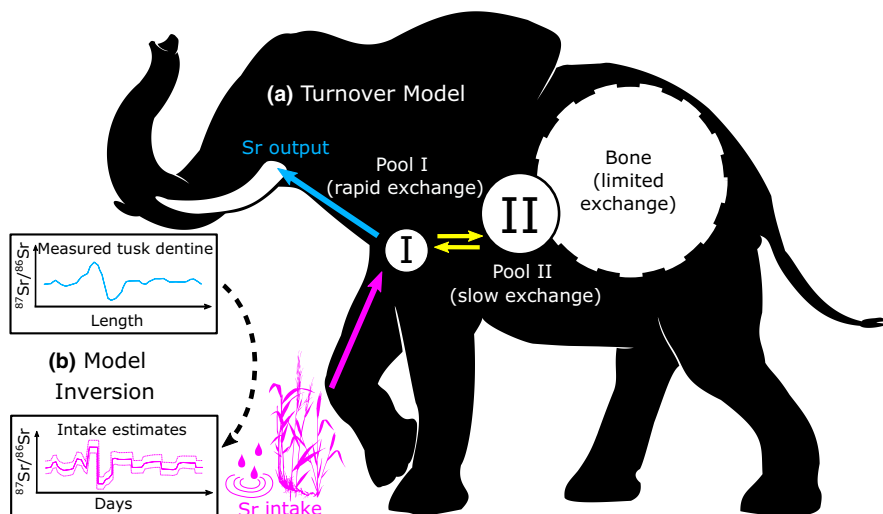
(Figure 1a). The resultant dentine powder was dissolved and analysed using the solution method (Data S1).

2.2 | Model description

Strontium is known to be a substitute for calcium in mineralized tissues such as bone, dentine and enamel. Studies of calcium metabolism suggested that there are at least two distinct pools of calcium in the body that participate in the turnover process (Braithwaite & Riazuddin, 1971; Meiggs, 2007). One is a rapidly exchanging pool (e.g. serum and liver); the other is a slowly exchanging pool (e.g. muscles and other internal organs) that is linked to the immense bone reservoir comprising over 99% of Ca and Sr in the animal (Meiggs, 2007). We assume that the rapidly exchanging pool (Pool I) is the central pool of exchange where Ca/Sr intake, output and exchange with the slowly exchanging pool (Pool II) take place, while Pool II includes

the chemically active subset of the immense bone pool (Figure 2a; Meiggs, 2007). We also assume that (1) there is no change in dietary Sr intake, concentration or Sr/Ca over time, (2) both pools are at steady state with respect to mass (no change in the pool sizes, i.e. Sr intake and excretion rates are equal), (3) both pools are isotopically well mixed, and (4) there is no ^{87}Sr fractionation within the animal (Flockhart et al., 2015; Lewis et al., 2017). With these assumptions, we use the constants P_n and F_n to represent the mass (mg) of and mass flux (mg/day) into/out of Pool n (respectively) and variable R_n to represent the Sr ratio of Pool/source n.

For P_{II}, the partial differential equation of its isotope ratio can be written as:

$$\frac{\partial R_{II}}{\partial t} = -\frac{F_{II}}{P_{II}}(R_{II} - R_I),$$ (1)

where $\frac{F_{II}}{P_{II}}$ is the first-order isotope reaction rate constant (λ) of P_{II} under a steady state assumption (Martínez del Rio & Carleton, 2012), which

can be used to derive half-life (e.g. Cerling, Ayliffe, et al., 2007; Tieszen et al., 1983):

$$t_{1/2} = \frac{\ln(2)}{\lambda}. \tag{2}$$

Similar to Equation (1), the partial differential equation of the isotope ratio of P_I can be written as:

$$\frac{\partial R_I}{\partial t} = -\frac{F_{in}}{P_I}(R_I - R_{in}) - \frac{F_{II}}{P_I}(R_I - R_{II}), \tag{3}$$

where $\frac{\partial R_I}{\partial t}$ is determined by the dynamic relationships between R_I, R_{in} and R_{II}, and the two first-order reaction rate constants $\frac{F_{in}}{P_I}$ and $\frac{F_{II}}{P_I}$, reflecting the processes of dietary intake and the exchange with P_{II}. Following Equation (2), each process here has a half-life derived from its reaction rate constant. For simplicity, the rate constants $\frac{F_{in}}{P_I}$, $\frac{F_{II}}{P_I}$ and $\frac{F_{II}}{P_{II}}$ will be referred to as a, b, c, respectively. Note that the rate constants have shared terms and are expected to show interactions. The rate constants can be further consolidated into two physiological parameters: the flux ratio $\frac{F_{in}}{F_{II}} = \frac{a}{b}$ and the pool ratio $\frac{P_I}{P_{II}} = \frac{c}{b}$, which are ultimately the independent terms of the turnover process.

Unlike enamel, tusk dentine is not affected by maturation averaging during its formation and unlike bone, it is not remodelled once it is formed (Boyde & Jones, 1972; Hillson, 2005; Passey & Cerling, 2002; Smith, 1998; Suga, 1982). Therefore, we assume that R_I is directly recorded in tusk dentine. Because the rate of dentine growth (micron/day) may vary from day to day, we consider that dentine formation rate at time step t is drawn from a normally distributed random variable. To make a quantitative correspondence between R_I at time step t (days) and measured $^{87}Sr/^{86}Sr$ at tusk dentine length R_I (micron), the length at time step t can be expressed using a cumulative function of growth rates:

$$l_t = \sum_1^t Rate_t. \tag{4}$$

At last, the Sr ratio measurement at length l is an average between lengths $l - \frac{1}{2}l_a$ and $l + \frac{1}{2}l_a$, where l_a is the sampling length associated with the analytical method. Therefore, the corresponding time steps of data integration at length l can be written as $t_{l+\frac{1}{2}l_a} - t_{l-\frac{1}{2}l_a}$. The full

correspondence between the average $^{87}Sr/^{86}Sr$ measured at length l (R_l^{avg}) and the $^{87}Sr/^{86}Sr$ time series of P_I ($R_{l,t}$) can be written as an unweighted average of the latter:

$$R_l^{avg} = \frac{1}{t_{l+\frac{1}{2}l_a} - t_{l-\frac{1}{2}l_a}} \sum_{t_{l-\frac{1}{2}l_a}}^{t_{l+\frac{1}{2}l_a}} R_{l,t}. \tag{5}$$

2.3 | Model components

We implement the turnover model to simulate a length-series of tusk Sr isotope ratios that can be compared directly with LA-ICP-MS data and use the model in three applications (Table 1). First, we use an assumed (stepwise) pattern of dietary change and tusk data documenting Misha's relocation to calibrate the model's rate constants. Second, we conduct a fidelity test using the calibrated rate constants to estimate Misha's $^{87}Sr/^{86}Sr$ intake time series directly from the measured data and compare the result with the assumed pattern of dietary change. Lastly, the model is used in a case study to reconstruct the intake $^{87}Sr/^{86}Sr$ time series of a woolly mammoth from measured tusk dentine $^{87}Sr/^{86}Sr$ data. We also explore the influence of the turnover parameter values on the shape of the turnover curve by building a forward model with synthetic intakes and turnover rate constants (Section 5, Data S1).

In each model study, we use a Markov chain Monte Carlo (MCMC) method to generate samples from the posterior distribution of all model parameters conditioned on the measured dentine $^{87}Sr/^{86}Sr$ series. The model described above is coded in the JAGS (Just Another Gibbs Sampler) syntax, which is implemented in R version 4.0.5 (R Core Team, 2023), using the 'rjags' package with the standalone JAGS encoder (Plummer, 2021). Five chains are run in parallel, and the minimum number of iterations is set at 5000 to ensure model convergence, with the first 2000 iterations as burn-ins. Average run time varies between 28 and 50h, depending on the number of time steps (t, days) incorporated in the time series simulation. Convergence is assessed visually via trace plots and with reference to the convergence factor 'rhat' (Gelman & Rubin, 1992) and effective sample sizes reported by the 'rjags' package. For each model parameter, its posterior density is summarized via the Kernel

TABLE 1 Summary of the four model components (columns) in the strontium turnover model and the three ways the model is used inversely (rows) in this study; bold text indicates the model component targeted for optimization in each study.

Model study	Model components			
	Intake $^{87}Sr/^{86}Sr$ time series	Turnover rate parameters	Dentine growth simulation	Sampling simulation
1. Calibration: estimate rate constants	Step function	**A fast central pool and a slow peripheral pool, both with uninformative priors**	Misha's dentine growth	Misha's LA-ICP-MS
2. Fidelity test: estimating intake time series of Misha	**Uninformative random walk**	Posterior from Calibration	Misha's dentine growth	Misha's LA-ICP-MS
3. Case study: estimating $^{87}Sr/^{86}Sr$ intake time series of Mammoth dentine	**Uninformative random walk**	Posterior from Calibration scaled to Mammoth's BM	Mammoth dentine growth	Mammoth LA-ICP-MS

density estimation function 'density' in the R package 'stats' with default settings. For selected parameters, posterior density summaries such as the maximum a posteriori estimate (MAP), and the 89% highest density interval (89% HDI, following McElreath, 2018) are reported using functions in the R package 'bayestestR' (Makowski et al., 2019).

2.4 | Parameter calibration

In the parameter calibration study, the $^{87}Sr/^{86}Sr$ intake series is modelled as a step function (Table 2), with values for the pre- and post-move intake (R_{pri} and R_{aft}) at each time step drawn from normal distributions centered on the measured $^{87}Sr/^{86}Sr$ values at the beginning and end of Misha's dentine (Section 2, Data S1). The prior parameter range for the date of the move (*Switch*, Table 2) in the intake time series is informed by both her dentine growth rate and $^{87}Sr/^{86}Sr$ values of her dentine (Section 2, Data S1). The rate constants a and c

are given uninformative priors, while b is given the prior constraint: $b < a$ (Table 2), informed by the literature showing that the central pool (P_I) exchanges faster than the peripheral pool (P_{II}) (Braithwaite et al., 1969; Braithwaite & Riazuddin, 1971). In all model studies, the initial condition for each pool is drawn from a normal distribution centred on the initial dietary intake value. Tusk dentine growth rate parameters are from Uno, Fisher, Schuster, et al. (2020). Length of averaging (l_a, in microns, Table 2) is calculated based on a 50-point averaging function of the raw LA-ICP-MS data. R_l^{mea} and σ_l^{mea} are the 50-point average values and their respective standard deviations. Prior parameters of the precision terms for R_{pri} and R_{aft} have been prescribed based on their variance in the raw LA-ICP-MS data. Prior parameters of the precision terms for $R_{I,t}$ and $R_{II,t}$ have been prescribed to reflect their relative uncertainties compared to R_{pri} and R_{aft} in the turnover process. We test model sensitivities to prior parameterizations, including R_{aft} value, the date of relocation and prior constrains on the rate constants (results presented in Section 4, Data S1).

TABLE 2 Deterministic/stochastic relationships, prior distributions and associated parameter values of the Sr turnover model used in the parameter calibration step of the framework.

Model components	Deterministic/stochastic relationships	Parameter values	Data type (unit)
Intake	$R_{pri_{mod}} \sim N\left(R_{pri}, \tau_{R_{pri}}\right)$	$R_{pri} = 0.706$	$^{87}Sr/^{86}Sr$ (NA)
	$\tau_{R_{pri}} \sim Gamma\left(\tau_{R_{pri}}shp, \tau_{R_{pri}}rate\right)$	$\tau_{R_{pri}}shp = 100;$ $\tau_{R_{pri}}rate = 2 \times 10^{-6}$	Precision (NA)
	$R_{aft_{mod}} \sim N\left(R_{aft}, \tau_{R_{aft}}\right)$	$R_{aft} = 0.711$	$^{87}Sr/^{86}Sr$ (NA)
	$\tau_{R_{aft}} \sim Gamma\left(\tau_{R_{aft}}shp, \tau_{R_{aft}}rate\right)$	$\tau_{R_{aft}}shp = 100;$ $\tau_{R_{aft}}rate = 2 \times 10^{-5}$	Precision (NA)
	$Rin_{pri} \sim N\left(R_{pri_{mod}}, \tau_{R_{pri}}\right)$	$pri = 1, ..., Switch$	$^{87}Sr/^{86}Sr$ (NA)
	$Rin_{aft} \sim N\left(R_{aft_{mod}}, \tau_{R_{aft}}\right)$	$aft = Switch + 1, ..., t$	$^{87}Sr/^{86}Sr$ (NA)
	$Switch \sim Cat(p_1 : p_k)$	$p_1 = 83; p_k = 87$	Date (day)
Turnover	$R_{I,1} \sim N\left(R_{pri_{mod}}, \tau_{RI}\right)$		$^{87}Sr/^{86}Sr$ (NA)
	$\tau_{RI} \sim Gamma\left(\tau_{RI}shp, \tau_{RI}rate\right)$	$\tau_{RI}shp = 100;$ $\tau_{RI}rate = 5 \times 10^{-6}$	Precision (NA)
	$R_{I,t} = R_{I,t-1} + b\left(R_{II,t-1} - R_{I,t-1}\right) + a\left(Rin_{t-1} - R_{I,t-1}\right)$		$^{87}Sr/^{86}Sr$ (NA)
	$a \sim Unif(0,1)$		Reaction rate (day^{-1})
	$b = b_{coef}a$		
	$b_{coef} \sim Unif(0,1)$		Reaction coefficient (NA)
	$R_{II,1} \sim N\left(R_{pri_{mod}}, \tau_{RII}\right)$		$^{87}Sr/^{86}Sr$ (NA)
	$\tau_{RII} \sim Gamma\left(\tau_{RII}shp, \tau_{RII}rate\right)$	$\tau_{RII}shp = 100;$ $\tau_{RII}rate = 5 \times 10^{-7}$	Precision (NA)
	$R_{II,t} = R_{II,t-1} + c\left(R_{I,t-1} - R_{II,t-1}\right)$		$^{87}Sr/^{86}Sr$ (NA)
	$c \sim Unif(0,1)$		Reaction rate (day^{-1})
Dentine growth	$Rate_t \sim N(\mu, \sigma)$	$\mu = 14.7, \sigma = 0.8$	Growth (μm day^{-1})
Sampling	$R_l^{avg} = \frac{1}{t_{l+\frac{1}{2}l_a} - t_{l-\frac{1}{2}l_a}} \sum_{t_{l-\frac{1}{2}l_a}}^{t_{l+\frac{1}{2}l_a}} R_{I,t}$	$l_a = 52.4$	Sampling window (μm)
	$R_l^{mea} \sim N\left(R_l^{avg}, \sigma_l^{mea}\right)$	$R_l^{mea} = mean\left(R_{l+\frac{1}{2}l_a}^{raw} : R_{l-\frac{1}{2}l_a}^{raw}\right),$ $\sigma_l^{mea} = sd\left(R_{l+\frac{1}{2}l_a}^{raw} : R_{l-\frac{1}{2}l_a}^{raw}\right)$	$^{87}Sr/^{86}Sr$ (NA)

Note: Tusk dentine growth rate is from Uno, Fisher, Schuster, et al. (2020).

2.5 | Fidelity test: Estimating ^{87}Sr/^{86}Sr intake series of Misha

To test the fidelity of the BITS framework, we use the rate constants and Misha's dentine measurements to estimate Misha's ^{87}Sr/^{86}Sr intake series. ^{87}Sr/^{86}Sr intake (Rin_t) is modelled as a random walk (Table 3). The initial value of the intake time series (Rin_{int}) is given a weakly informative prior following a normal distribution with a generic mean and an inflated σ (Table 3). The change in Rin_t at each timestep is a random variable drawn from a Cauchy distribution with a scale parameter modelled with a Gamma distribution (Table 3). A Cauchy error term is selected over a normal random variable (Section 4.4, Data S1) to accommodate possible abrupt changes in ^{87}Sr/^{86}Sr, for example when an animal crosses discrete geological boundaries in the real world. To avoid abrupt changes that are beyond the realistic gradients of ^{87}Sr/^{86}Sr on land, the per-step change is limited to ±0.006 (Table 3). We test model sensitivity to the Cauchy scale parameter τ_{Rin} rate (results presented in Section 4.3, Data S1). Due to the highly unusual step function in Misha's ^{87}Sr/^{86}Sr intake and its expected deviation from the Cauchy distribution, we found it necessary to tune the prior of the Cauchy scale parameter τ_{Rin} rate to avoid substantial mismatch between the turnover model posterior parameter distributions in the fidelity and calibration studies (more in the Discussion). In this fidelity test, parameters a, b and c are sampled from the posterior of the calibration study and parameters of dentine growth and measured dentine ^{87}Sr/^{86}Sr are the same as in Table 2.

2.6 | Case study: Estimating ^{87}Sr/^{86}Sr intake series of an Alaskan mammoth

To demonstrate the utility of the BITS framework, we use a subset of the LA-ICP-MS derived ^{87}Sr/^{86}Sr data of a Woolly Mammoth (*Mammuthus primigenius*) tusk found in Alaska (Wooller et al., 2021) and estimate the animal's ^{87}Sr/^{86}Sr intake series. Sensitivity tests show that, unlike in the fidelity test, the turnover rates are not very sensitive to

the prior on Cauchy scale parameter τ_{Rin} rate (Section 4.3, Data S1). Therefore, τ_{Rin} rate = 1×10^{-7} is chosen (Table 4), which is near the centre of the tested range and accommodates a range of step sizes that are observed in bioavailable Sr isoscapes. Turnover model parameters a, b and c are first sampled from the posterior obtained in the calibration study, then scaled using expected allometric relationships between isotopic turnover rates and body mass. We assume that the rate constant linked to the rapidly exchanging pool (parameter a) is not affected by body mass (Thomas & Crowther, 2015), whereas those linked to the slowly exchanging pool (parameters b and c) scale negatively (with an exponent of −0.19) with body mass (Table 4, Thomas & Crowther, 2015). The body mass variables of both Misha and the Woolly Mammoth are modelled using normal distributions with parameters informed by the species and sex of each (Larramendi, 2015). Parameters of dentine growth are calculated using dentine lengths and annual markers (Wooller et al., 2021). To better characterise data uncertainty and reduce computational demand, we apply a 500-micron averaging window (l_{am}) to the raw data (Table 4), which also mimics an dentine series generated by more conventional sampling techniques such as micromilling (e.g. Miller et al., 2022; Uno, Fisher, Schuster, et al., 2020). Dentine ^{87}Sr/^{86}Sr means and standard deviations are calculated based on the 500-micron averaging window (see model code in Yang, 2023).

3 | RESULTS

3.1 | LA-ICP-MS results and parameter calibration

Prior to the move, the baseline mean ^{87}Sr/^{86}Sr from the CA portion of Misha's tusk is ca. 0.706 (Figure 3a), which falls just out of the range of published surface water samples from the Sacramento-San Joaquin delta (ca. 0.7061 to 0.7073) (Ingram & Weber, 1999). No feed sample is available from the area. After the move and at dentine distances ca. 17,000 microns from the pulp cavity, tusk ^{87}Sr/^{86}Sr rises quickly to ca. 0.709, followed by a long-term increase at dentine distances <17,000 microns from the

TABLE 3 Deterministic/stochastic relationships, prior distributions and associated parameter values of the Sr turnover model used in the fidelity test of the framework.

Model components	Deterministic/stochastic relationships	Parameter values	Data type (unit)
Intake	$Rin_{int} \sim N\left(R_{int}, \sigma_{Rint}\right)$	Rin_{int} = 0.710; σ_{Rint} = 0.01	^{87}Sr/^{86}Sr (NA)
	$Rin_1 \sim N\left(Rin_{int}, \tau_{Rin}\right)$		^{87}Sr/^{86}Sr (NA)
	$\tau_{Rin} \sim Gamma\left(\tau_{Rin}shp, \tau_{Rin}\,rate\right)$	$\tau_{Rin}shp$ = 100; $\tau_{Rin}\,rate$ = 2.5×10^{-8}	Precision (NA)
	$Rin_t \sim Cauchy\left(Rin_{t-1}, \tau_{Rin}\right)$	$\mid Rin_t - Rin_{t-1} \mid$ < 0.006	^{87}Sr/^{86}Sr (NA)
Turnover	Same as Table 2	Parameters a, b, and c are sampled from the posterior of the calibration study	Reaction rate (day^{-1})
Dentine growth & Sampling	Same as Table 2		

TABLE 4 Deterministic/stochastic relationships, prior distributions and associated parameter values of the Sr turnover model used in the case study.

Model components	Deterministic/stochastic relationships	Parameter values	Data type (unit)
Intake	Same as Table 3, except for the Cauchy scale parameter below		
	$\tau_{Rin} \sim Gamma\,(\tau_{Rin}shp, \tau_{Rin}\,rate)$	$\tau_{Rin}shp = 100;$ $\tau_{Rin}\,rate = 1 \times 10^{-7}$	Precision (NA)
Turnover	Same as Table 2, with additional relationships below	a, b, and c are sampled from the posterior of the calibration	Reaction rate (day^{-1})
	$a.m = a(BM_{mamm}/BM_{Misha})^{scla}$ $b.m = b(BM_{mamm}/BM_{Misha})^{sclbc}$ $c.m = c(BM_{mamm}/BM_{Misha})^{sclbc}$	$sclx$: exponents for allometric scaling with body mass	Reaction rate (day^{-1})
	$BM_{Misha} \sim N\,(\mu, \sigma)$	$\mu = 3000, \sigma = 150$	Body mass (kg)
	$BM_{Mamm} \sim N\,(\mu, \sigma)$	$\mu = 7500, \sigma = 500$	Body mass (kg)
	$scla \sim N\,(\mu, \sigma)$	$\mu = 0, \sigma = 0.05$	Scaling factor (NA)
	$sclbc \sim N\,(\mu, \sigma)$	$\mu = -0.19, \sigma = 0.05$	Scaling factor (NA)
Dentine growth	$Rate_t \sim N\,(\mu, \sigma)$	$\mu = 169, \sigma = 27$	Growth (µm day^{-1})
Sampling	$R_l^{avg} = \frac{1}{t_{l+\frac{1}{2}l_{am}} - t_{l-\frac{1}{2}l_{am}}} \sum_{t_{l-\frac{1}{2}l_{am}}}^{t_{l+\frac{1}{2}l_{am}}} R_{l,t}$ $R_l^{mea} \sim N\,(R_l^{avg}, \sigma_l^{mea})$	$l_{am} = 500$ $R_l^{mea} = mean\left(R_{l+\frac{1}{2}l_{am}}^{raw} : R_{l-\frac{1}{2}l_{am}}^{raw}\right)$ $\sigma_l^{mea} = sd\left(R_{l+\frac{1}{2}l_{am}}^{raw} : R_{l-\frac{1}{2}l_{am}}^{raw}\right)$	Sampling window (µm) ^{87}Sr/^{86}Sr (NA)

Note: Dentine growth rate is calculated from Wooller et al. (2021).

pulp cavity (Figure 3a). Toward the end of the transect, the tusk ^{87}Sr/^{86}Sr reaches ca. 0.711, which falls within the range of measured and published values of feed and water (between ca. 0.7080 and 0.7132, Figure 3b). The data generated by the laser ablation method are consistent with those from the micromill via the solution method (Figure S2, Data S1). A numeric model estimating the daily Sr mass intake (Figure 3b; Section 3, Data S1) shows that elephant feed (hay, pellets, and supplements) was Misha's primary Sr source after the move.

Tusk ^{87}Sr/^{86}Sr values increase continuously throughout most of the turnover event but show a transient excursion toward lower values early in the change (Figure 3a). We note that the excursion is in close proximity to a crack in the tusk dentine slab that may have introduced contamination along the laser transect (Data S1). The excursion is also inconsistent with the step-function of the modelled intake and the steady-state turnover process. Given this, and to avoid potential errors in model calibration, the data associated with the excursion are excluded from subsequent analyses (Figure 3c). From the onset of ^{87}Sr/^{86}Sr increase to the pulp cavity surface, the distance on slab M640b is 18.14 mm, representing the total number of days Misha lived in Utah (1236 days). This yields an average dentine growth rate $Rate_t$ at 14.7 ± 0.8 microns per day (Uno, Fisher, Schuster, et al., 2020).

All rate constants show clear central tendencies in the posterior distributions obtained by inverting the 'calibration' version of the model conditioned on the tusk ^{87}Sr/^{86}Sr data (Figure 3d). Parameter a shows an MAP at 0.0169, which translates to a half-life of ca. 41 days for turnover of P_I via the intake flux (Table 5). Parameter c

shows an MAP at 0.0041, giving a half-life of ca. 170 days for the slow-turnover pool (Table 5). The bivariate posterior density of the pool ratio (P_I/P_{II}) and flux ratio (F_{in}/F_{II}) shows a single peak at ca. 0.2 for pool ratio and ca. 1.05 for flux ratio, with a weak correlation between the two variables (Figure 3e).

3.2 | Fidelity test: Estimating ^{87}Sr/^{86}Sr intake series of Misha

The model-estimated intake ^{87}Sr/^{86}Sr time series based on Misha's LA-ICP-MS data shows good agreement with the intake estimated using the more prescriptive prior in the calibration analysis (Section 2.4). The estimated date of the relocation is almost identical to that estimated during calibration. The estimated magnitude of change in intake ^{87}Sr/^{86}Sr (ca. +0.0045) is slightly smaller than that estimated during calibration (ca. +0.0050), and the fidelity test suggests a brief interval of more gradual increase immediately prior to the modelled date of relocation (Figure 4). For most of the post-relocation series, the estimated intake ^{87}Sr/^{86}Sr values agree well with those of the calibration and display local variations that are consistent with the measured ^{87}Sr/^{86}Sr series (e.g. a transient rise and fall around day 200, and a step up after day 600 Figure 4a). After tuning the prior distribution of the precision parameter τ_{Rin} using its hyper parameter $\tau_{Rin}rate = 2.5 \times 10^{-8}$, the posterior distribution for turnover parameter a is equivalent to that obtained in the calibration (Figure 4b).
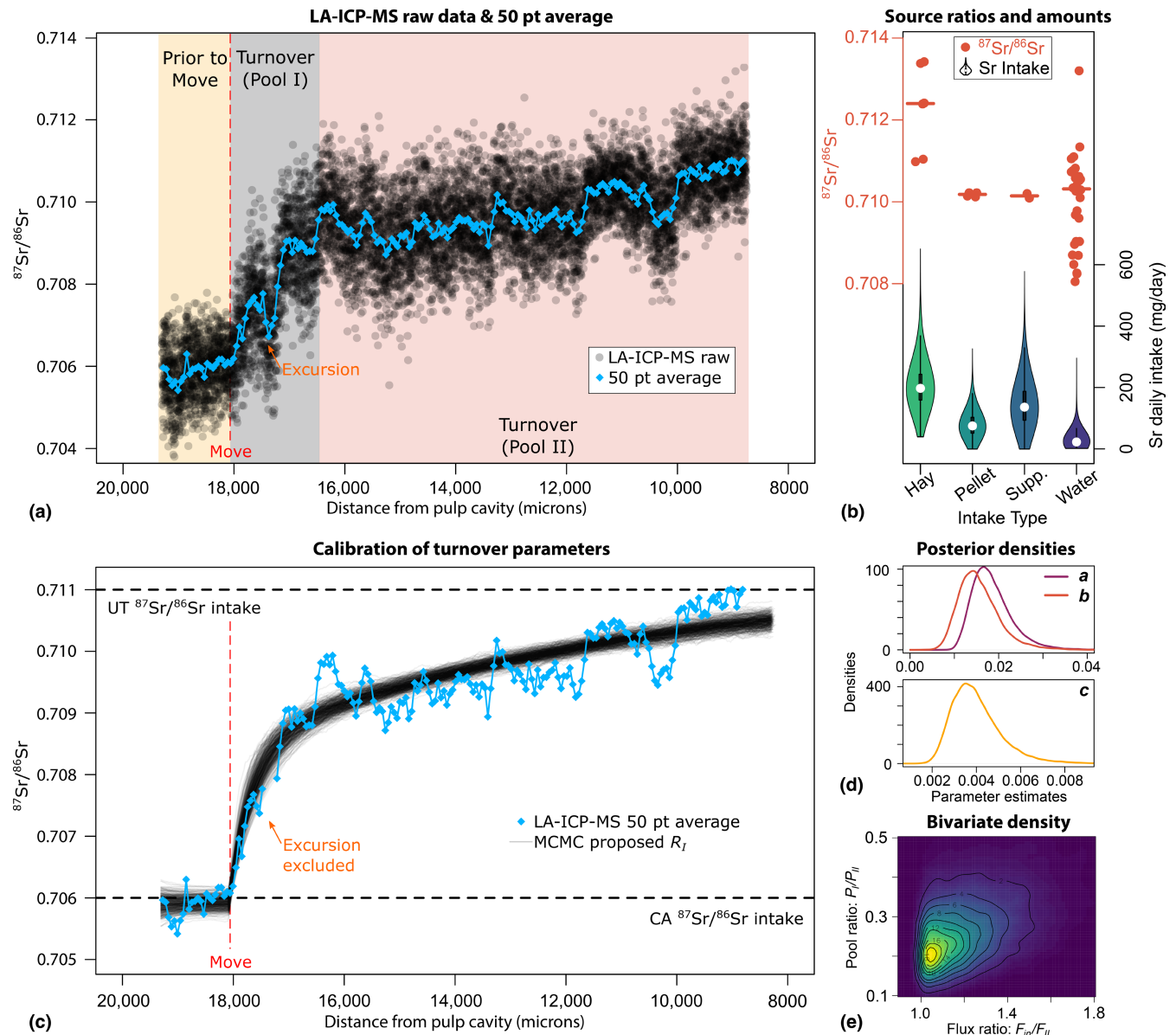
FIGURE 3 (a) $^{87}Sr/^{86}Sr$ raw data measured by laser ablation inductively coupled plasma mass spectrometry (LA-ICP-MS, black dots), the 50-point average series (blue diamonds and lines), plotted with their associated distance (micron) from the pulp cavity of Misha's dentine (x-axis). The vertical dashed line marks the approximate distance associated with the move. (b) $^{87}Sr/^{86}Sr$ of feed (hay, pellet, and supplements) and water measured by the solution method (orange), and their modelled Sr daily intake amount (mg/day). (c) MCMC proposed R_I time series (black lines) based on the turnover model and their fit onto the LA-ICP-MS 50-point average series (blue diamonds and lines). (d) Posterior densities of rate constants a, b, and c. (e) Bivariate density heatmap and contours of the two independent variables of the turnover model: Pool ratio and Flux ratio.

3.3 | Case study: Estimating $^{87}Sr/^{86}Sr$ intake series of an Alaskan mammoth

The selected LA-ICP-MS transect represents ca. 2 years of adult life for the male Woolly Mammoth (Wooller et al., 2021). The dentine data show three clusters of $^{87}Sr/^{86}Sr$ with gradual transitions between each cluster (Figure 5a,d). The sequence starts with dentine clustering around the high $^{87}Sr/^{86}Sr$ values at ca. 0.712, then transitions to the intermediate values at ca. 0.7105, and subsequently to the low ones at ca. 0.709, and finally ends back in the high $^{87}Sr/^{86}Sr$ values (Figure 5a). By contrast, the estimated intake $^{87}Sr/^{86}Sr$ series show a much wider range of values from ca. 0.707 to 0.713, and four

clusters instead of three (Figure 5b,d). In addition, the estimated intake $^{87}Sr/^{86}Sr$ time series displays abrupt changes in $^{87}Sr/^{86}Sr$, which deviate from the more gradual changes seen in dentine measurements (Figure 5b). The posterior of the rate constant $a.m$ (Table 4; Figure 5c) has shifted to higher values than the prior (parameter a in the calibration), with an MAP at 0.0225 (Figure 5c) that translates into a half-life of ca. 30.9 days for P_I in response to intake (Table 5). Parameter $c.m$ shows a MAP at 0.0034 (Figure 5c) that translates into a P_{II} half-life of ca. 202 days (Table 5). The bivariate density of pool ratio (P_I/P_{II}) and flux ratio (F_{in}/F_{II}) shows a single peak at ca. 0.19 for pool ratio (lower than the calibration), and at ca. 1.28 for flux ratio (higher than the calibration, Figure 5e).

TABLE 5 Summary statistics of model parameters for the proboscidean individuals investigated in this study.

Model parameter	Parameter description (unit)	Posterior: Misha (*Loxodonta africana*)	Posterior: Alaskan mammoth (*Mammuthus primigenius*)
P_I/P_{II}	Pool ratio, central pool/peripheral pool (NA)	MAP: 0.246 89% HDI: 0.135–0.425	MAP: 0.187 89% HDI: 0.124–0.335
F_{in}/F_{II}	Flux ratio, intake flux/peripheral pool flux (NA)	MAP: 1.03 89% HDI: 1.00–1.47	MAP: 1.28 89% HDI: 1.09–1.64
a	Reaction rate from intake to P_I (day^{-1})	MAP: 0.0169 89% HDI: 0.0122–0.0253	MAP: 0.0225 89% HDI: 0.0161–0.0298
b	Reaction rate from P_{II} to P_I (day^{-1})	MAP: 0.0141 89% HDI: 0.0086–0.0227	MAP: 0.0164 89% HDI: 0.0105–0.0233
c	Reaction rate from P_I to P_{II} (day^{-1})	MAP: 0.0041 89% HDI: 0.0025–0.0060	MAP: 0.0034 89% HDI: 0.0023–0.0053
$ln(2)/a$	Half-life associated with a (days)	MAP: 41.0 89% HDI: 27.4–56.8	MAP: 30.9 89% HDI: 23.3–43.1
$ln(2)/b$	Half-life associated with b (days)	MAP: 49.3 89% HDI: 30.6–80.8	MAP: 42.2 89% HDI: 29.7–66.1
$ln(2)/c$	Half-life associated with c (days)	MAP: 170 89% HDI: 116–277	MAP: 202 89% HDI: 130–300

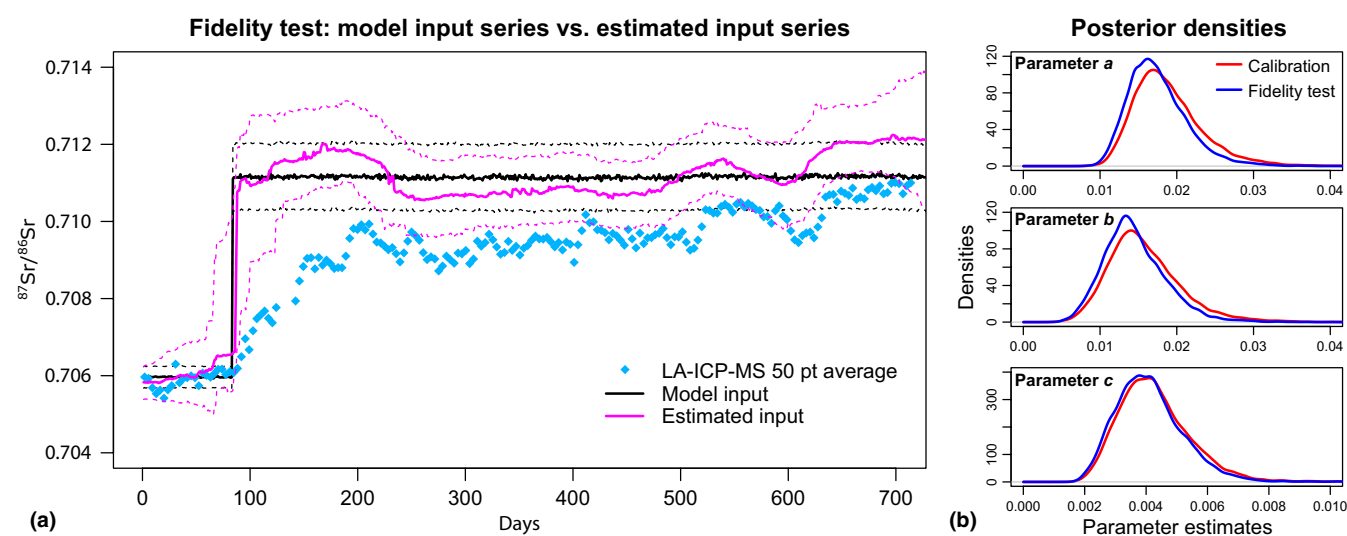*Note*: HDI, highest density interval; MAP, maximum a posteriori estimate.

FIGURE 4 Results of the fidelity test comparing estimated intake ^{87}Sr/^{86}Sr time series to model input (posterior distribution of the calibration study). Blue diamonds are 50-point average series from laser ablation inductively coupled plasma mass spectrometry (LA-ICP-MS); the black solid line represents maximum a posteriori estimates (MAPs) of model input. The magenta solid line represents MAPs of estimated intake in the fidelity test. Dashed lines represent 89% highest density intervals. (b) Comparisons of posterior densities of the three rate constants a, b and c between the fidelity test and the calibration (Figure 3d).

4 | DISCUSSION

4.1 | Characteristics of the BITS framework

The Sr isotope incorporation pattern, as recorded in Misha's dentine, follows a two-compartment turnover process similar to the calcium metabolism in sheep (Braithwaite et al., 1969; Braithwaite & Riazuddin, 1971). The two-compartment turnover process can also be described using the reaction progress (RP) model (Cerling, Ayliffe, et al., 2007), which is particularly useful in detecting the number of

pools in an isotope turnover system (Cerling, Bowen, et al., 2007; Section 6, Data S1). The advantages of the BITS model over the RP model are the explicit and mechanistic representations of the isotope exchanges between the pools, the more appropriate parameterization of the model and the ability to provide credible intervals of the modelled isotope input time series with Bayesian statistics (see a detailed comparison in Section 6, Data S1). Results from the BITS forward model show that the combination of pool ratio and flux ratio can accommodate a variety of shapes in the turnover curve (Section 5, Data S1). The Sr isotope turnover process is notably different
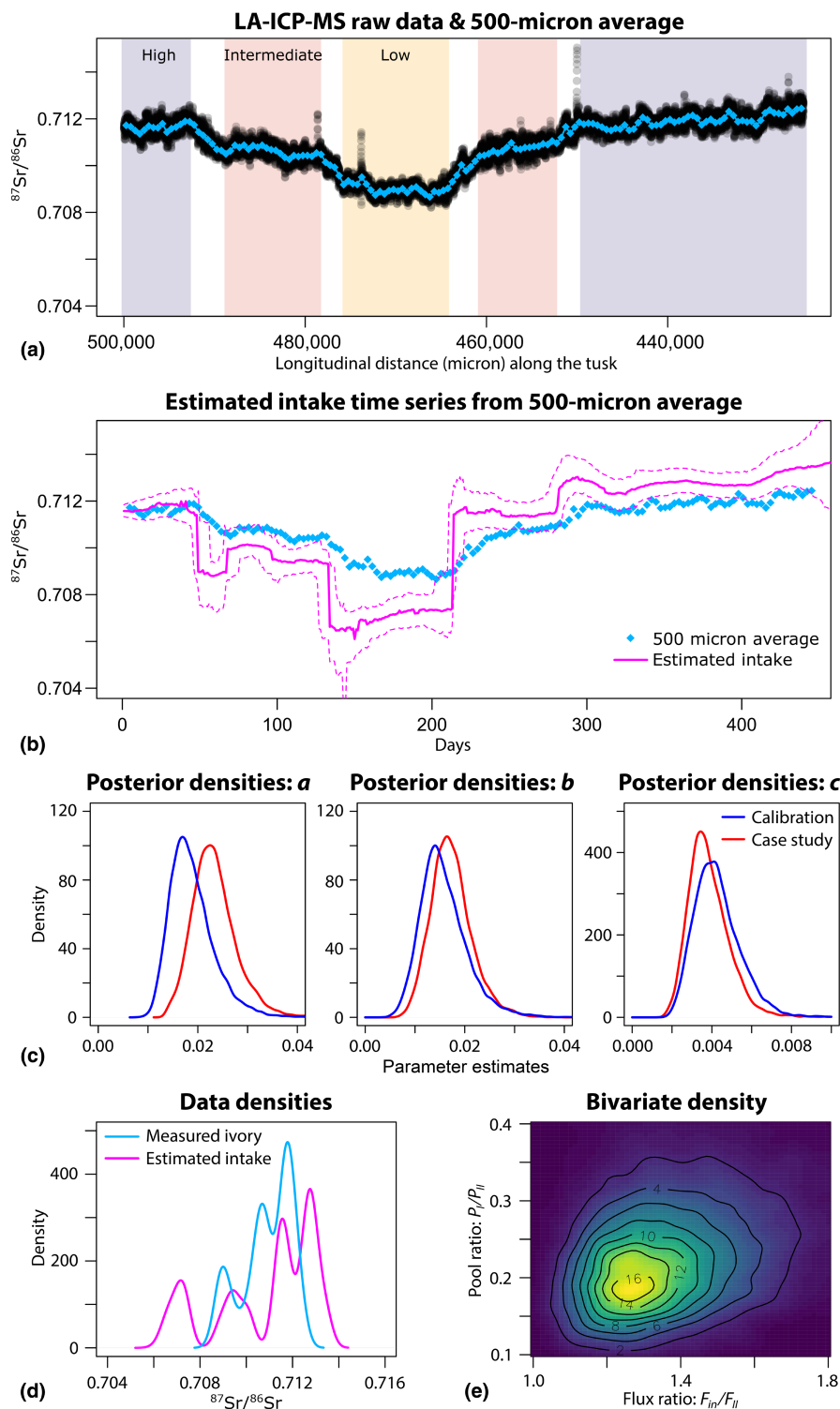
FIGURE 5 Results of the case study using selected $^{87}Sr/^{86}Sr$ data of a woolly mammoth tusk (Wooller et al., 2021). (a) $^{87}Sr/^{86}Sr$ raw data measured by laser ablation inductively coupled plasma mass spectrometry (LA-ICP-MS, black dots), the 500-micron average series (light blue diamonds and lines), plotted with their associated longitudinal distance (micron) along the tusk. Coloured shadings indicate three clusters of $^{87}Sr/^{86}Sr$ measured in the dentine. (b) Model estimated $^{87}Sr/^{86}Sr$ input series based on LA-ICP-MS $^{87}Sr/^{86}Sr$ measurements. The magenta solid line represents maximum a posteriori estimates of estimated intake in the fidelity test. Dashed lines represent 89% highest density intervals. Blue diamonds are the same 500-micron average series used in panel (a). (c) Posterior densities of rate constants $a.m$, $b.m$ and $c.m$ in the case study (red curves) compared to those of parameters a, b and c in the calibration (blue curves, Figure 3d), respectively. (d) Comparing Kernel density estimates of the measured dentine series (light blue curve) and the model estimated intake series (magenta curve). (e) Bivariate density heatmap and contours of the pool ratio and the flux ratio of the case study mammoth.

from that of carbon and oxygen isotopes inferred from Misha's dentine, which is best represented by a one-compartment turnover with a short half-life at ca. 7–10 days (Uno, Fisher, Schuster, et al., 2020). The much slower turnover of both the central and the peripheral Sr pools suggests that Sr isotope data in incrementally grown tissues reflects a much longer time scale of integration than other isotope systems such as carbon and oxygen. This can directly impact data interpretation, in that synchronous changes in intake would lead to

lagged and smoothed expression in tissue Sr isotope data relative to that in fast-turnover systems (e.g. carbon or oxygen). The best way to account for such a potential bias is to use a modelling framework, such as BITS and the RP model (Cerling, Ayliffe, et al., 2007), to estimate the original isotope input time series.

In the fidelity test, the rate constants and the estimated input time series are sensitive to the hyper prior parameter τ_{Rin} *rate* of the intake time series (Section 4.3, Data S1). By contrast, little sensitivity

is found in the case study with the woolly mammoth. This is likely due to the extreme case of Misha's movement history and the associated $^{87}Sr/^{86}Sr$ change in her intake (a single step change), which deviates from the more stochastic variation expected in natural settings. In the case study, the model converged on slightly faster turnover rates than expected based on the scaling relationship with body mass. Although we cannot validate these parameters independently, this suggests the possibility that the BITS framework could help constrain turnover rates in extinct animals.

Our case study application shows that abrupt changes in $^{87}Sr/^{86}Sr$ intake, of the type that would be expected for an animal moving across geological boundaries, are consistent with measured dentine data that themselves exhibit gradual changes. We used the Cauchy distribution in modelling the input time series to accommodate such abrupt changes (see Section 4.4 in Data S1 for a comparison between different input time series structures), which appears to be an acceptable solution but could be replaced by other model forms that more accurately represent expected intake patterns for mobile animals (e.g. Wooller et al., 2021). The much wider range of estimated $^{87}Sr/^{86}Sr$ intake compared to measured dentine (Figure 5b,d) suggests that the input signal amplitude can be substantially attenuated by the turnover process in proboscideans. It further suggests the need to consider and correct for the effects of turnover on measured dentine $^{87}Sr/^{86}Sr$ series in order to generate robust reconstructions of animal movements and home ranges.

Our BITS framework makes an explicit link between time and tissue by simulating cumulative incremental growth. Although here we assume only stochastic variation in the growth rate of Misha's dentine, systematic variation in dentine growth rates, for example due to seasonality or stressors (e.g. Koch et al., 1989; Uno, Fisher, Schuster, et al., 2020; Wooller et al., 2021), can be accommodated in the cumulative function (Equation 4). The built-in averaging function (Equation 5) serves to perform data reduction and to simulate potential data averaging effects when sampling incremental tissues. As such, the framework incorporates important sources of uncertainties associated with the correspondence between the life history of the organism (e.g. measured in days) and data measured in the incremental tissue (e.g. measured in distance).

4.2 | Potential utility and future directions

Our BITS framework bridges the gap between environmental $^{87}Sr/^{86}Sr$ variations and data measured in dentine or other incrementally grown tissues. The model mathematically resolves the time scale of Sr isotopic integration and allows quantitative estimations of $^{87}Sr/^{86}Sr$ intake time series. The framework can be applied to micro-sampled records of dentine in other organisms following the workflow established in this study. Moreover, it can be coupled with upstream geospatial modelling frameworks that use $^{87}Sr/^{86}Sr$ to study animal mobility/migration ecology (e.g. Ma et al., 2020; Wunder, 2012). For example, the posterior of the estimated $^{87}Sr/^{86}Sr$ intake series, when coupled with movement models (e.g. Brennan et al., 2019; Sakamoto

et al., 2019; Trueman & St John Glew, 2019; Wooller et al., 2021), could be used to estimate individual home range or movement history. The modelling approach can be particularly powerful when coupled with additional tracers (e.g. carbon and oxygen isotopes; Kowalik et al., 2023; Miller et al., 2022; Wooller et al., 2021) to inform, for example seasonal residence patterns or the timing of migration. The generic isotope turnover processes and the BITS framework discussed here can be adapted to data for other isotope systems (with fractionations involved) or other organisms of interest (with additional turnover calibrations). Applications like these can improve the reliability of interpretations based on isotopic data in incremental tissues and expand our modelling toolkit to investigate, for example niche partitioning, life history traits, and behavioural patterns.

The BITS model of Sr isotope incorporation into tusk dentine involves simplifying assumptions which could be revisited in future studies. For example, the model does not consider variable Sr or Ca elemental concentrations or compositions of food and water separately (e.g. Ericson, 1989; Meiggs, 2007; Phillips & Koch, 2002; Weber et al., 2020) or represent non-steady state Sr or Ca mass balance scenarios that involve changing pool sizes or elemental fluxes, such as rapid growth or lactation that involve substantial exchange with the bone pool. Incorporation of such effects will help researchers accommodate environmental, physiological and ontogenic factors that may influence $^{87}Sr/^{86}Sr$ data interpretation in real-world systems. In addition, application of the model to other tissues, such as dental enamel, presents additional challenges due to time-averaging that occurs during tissue formation, and will require additional model components (e.g. Green et al., 2018; Passey & Cerling, 2002). Regardless of these limitations, the BITS framework is adaptable and could easily accommodate inclusion of these and other processes, expanding its utility. Our results also emphasize the importance of understanding isotope incorporation patterns before isotope data can be confidently interpreted. The decades-old appeals for conducting more laboratory experiments (Gannes et al., 1997) and developing more theoretical models (Martínez del Rio et al., 2009) still stand to this day.

AUTHOR CONTRIBUTIONS

Deming Yang conceived the modelling approach and developed the model code in discussion with the other authors. Gabriel J. Bowen assisted with the structure and statistics of the model. Kevin T. Uno, Nancy A. Carpenter and Thure E. Cerling conceived the project associated with Misha's relocation and secured the funding. Kevin T. Uno, Katya Podkovyroff and Diego P. Fernandez conducted the lab preparations and analyses. Deming Yang, Kevin T. Uno, Katya Podkovyroff and Diego P. Fernandez analysed the data. Deming Yang and Gabriel J. Bowen prepared a first version of the manuscript, and all authors contributed critically to successive drafts and gave final approval for publication.

ACKNOWLEDGEMENTS

CONFLICT OF INTEREST STATEMENT

The authors do not have a conflict of interest to declare.

PEER REVIEW

The peer review history for this article is available at https://www.webofscience.com/api/gateway/wos/peer-review/10.1111/2041-210X.14218.

DATA AVAILABILITY STATEMENT

The model code and associated data are available on Zenodo via https://doi.org/10.5281/zenodo.7741883 (Yang, 2023), and on GitHub via https://github.com/SPATIAL-Lab/BITS.

STATEMENT ON INCLUSION

Our study was based on a meta-analysis of primary data collected entirely within the United States. All authors were engaged early on with the research and study design to ensure that the diverse sets of perspectives they represent were considered from the onset of the project as an effort to support the inclusion of authors at different career stages. We recognize that more could have been done to engage authors and collaborators from other countries or regions of globe. We are planning to address the caveat of not including a plan to disseminate our work in other languages in future research.

ORCID

Deming Yang https://orcid.org/0000-0002-7719-6801
Gabriel J. Bowen https://orcid.org/0000-0002-6928-3104
Kevin T. Uno https://orcid.org/0000-0001-6882-0900
Diego P. Fernandez https://orcid.org/0000-0002-4727-5031
Thure E. Cerling https://orcid.org/0000-0002-3590-294X

REFERENCES

Bataille, C. P., Crowley, B. E., Wooller, M. J., & Bowen, G. J. (2020). Advances in global bioavailable strontium isoscapes. *Palaeogeography, Palaeoclimatology, Palaeoecology*, *555*, 109849. https://www.sciencedirect.com/science/article/pii/S0031018220302947

Bowen, G. J., & West, J. B. (2008). Isotope landscapes for terrestrial migration research. *Terrestrial Ecology*, *2*, 79–105. https://www.sciencedirect.com/science/article/pii/S1936796107000048

Boyde, A., & Jones, S. J. (1972). Scanning electron microscopic studies of the formation of mineralized tissue. In H. C. Slavkin & L. A. Bavetta (Eds.), *Developmental aspects of oral biology* (pp. 263–274). Academic Press.

Braithwaite, G. D., Glascock, R. F., & Riazuddin, S. (1969). Calcium metabolism in lactating ewes. *British Journal of Nutrition*, *23*(4), 827–834. https://www.cambridge.org/core/article/calcium-metabolism-in-lactating-ewes/F63F78D9D406450838D0F099E19D7DCD

Braithwaite, G. D., & Riazuddin, S. (1971). The effect of age and level of dietary calcium intake on calcium metabolism in sheep. *British Journal of Nutrition*, *26*(2), 215–225. https://www.cambridge.org/core/article/effect-of-age-and-level-of-dietary-calcium-intake-on-calcium-metabolism-in-sheep/A64BF36260D3AB82206F21E69AD2C7F7

Brennan, S. R., Cline, T. J., & Schindler, D. E. (2019). Quantifying habitat use of migratory fish across riverscapes using space-time isotope models. *Methods in Ecology and Evolution*, *10*(7), 1036–1047. https://doi.org/10.1111/2041-210X.13191

Brennan, S. R., Zimmerman, C. E., Fernandez, D. P., Cerling, T. E., McPhee, M. V., & Wooller, M. J. (2015). Strontium isotopes delineate fine-scale natal origins and migration histories of Pacific salmon. *Science Advances*, *1*(4), e1400124. https://doi.org/10.1126/sciadv.1400124

Britton, K., Le Corre, M., Willmes, M., Moffat, I., Grün, R., Mannino, M. A., Woodward, S., & Jaouen, K. (2020). Sampling plants and malacofauna in ^{87}Sr/^{86}Sr bioavailability studies: Implications for isoscape mapping and reconstructing of past mobility patterns. *Frontiers in Ecology and Evolution*, *8*. https://doi.org/10.3389/fevo.2020.579473

Carter, W. A., Bauchinger, U., & McWilliams, S. R. (2019). The importance of isotopic turnover for understanding key aspects of animal ecology and nutrition. *Diversity*, *11*(5), 84. https://www.mdpi.com/1424-2818/11/5/84

Cerling, T. E., Ayliffe, L. K., Dearing, M. D., Ehleringer, J. R., Passey, B. H., Podlesak, D. W., Torregrossa, A.-M., & West, A. G. (2007). Determining biological tissue turnover using stable isotopes: The reaction progress variable. *Oecologia*, *151*(2), 175–189. https://doi.org/10.1007/s00442-006-0571-4

Cerling, T. E., Bowen, G. J., Ehleringer, J. R., & Sponheimer, M. (2007). The reaction progress variable and isotope turnover in biological systems. *Terrestrial Ecology*, *1*, 163–171. https://www.sciencedirect.com/science/article/pii/S1936796107010111

Coelho, I., Castanheira, I., Bordado, J. M., Donard, O., & Silva, J. A. L. (2017). Recent developments and trends in the application of strontium and its isotopes in biological related fields. *TrAC Trends in Analytical Chemistry*, *90*, 45–61. https://www.sciencedirect.com/science/article/pii/S0165993616302953

Crowley, B. E., Miller, J. H., & Bataille, C. P. (2017). Strontium isotopes (^{87}Sr/^{86}Sr) in terrestrial ecological and palaeoecological research: Empirical efforts and recent advances in continental-scale models. *Biological Reviews*, *92*(1), 43–59. https://doi.org/10.1111/brv.12217

Dalerum, F., & Angerbjörn, A. (2005). Resolving temporal variation in vertebrate diets using naturally occurring stable isotopes. *Oecologia*, *144*(4), 647–658. https://doi.org/10.1007/s00442-005-0118-0

Ericson, J. E. (1989). Some problems and potentials of strontium isotope analysis for human and animal ecology. In P. W. Rundel, J. R. Ehleringer, & K. A. Nagy (Eds.), *Stable isotopes in ecological research* (pp. 252–259). Springer. https://doi.org/10.1007/978-1-4612-3498-2_14

Fisher, D. C., & Fox, D. L. (2007). Season of death of the dent mammoths. In R. H. Brunswig & B. L. Pitblado (Eds.), *From the dent prairie to the peaks of the Rockies: Recent Paleoindian research in Colorado* (pp. 123–153). University of Colorado Press.

Flockhart, D. T. T., Kyser, T. K., Chipley, D., Miller, N. G., & Norris, D. R. (2015). Experimental evidence shows no fractionation of strontium isotopes (^{87}Sr/^{86}Sr) among soil, plants, and herbivores: Implications

for tracking wildlife and forensic science. *Isotopes in Environmental and Health Studies*, 51(3), 372–381. https://doi.org/10.1080/10256016.2015.1021345

Gannes, L. Z., O'Brien, D. M., & Martínez del Rio, C. (1997). Stable isotopes in animal ecology: Assumptions, caveats, and a call for more laboratory experiments. *Ecology*, 78(4), 1271–1276. https://doi.org/10.1890/0012-9658%281997%29078%5B1271%3ASIIAEA%5D2.0.CO%3B2

Gelman, A., & Rubin, D. B. (1992). Inference from iterative simulation using multiple sequences. *Statistical Science*, 7(4), 457–472. https://doi.org/10.1214/ss/1177011136

Green, D. R., Smith, T. M., Green, G. M., Bidlack, F. B., Tafforeau, P., & Colman, A. S. (2018). Quantitative reconstruction of seasonality from stable isotopes in teeth. *Geochimica et Cosmochimica Acta*, 235, 483–504. http://www.sciencedirect.com/science/article/pii/S0016703718303284

Hillson, S. (2005). *Teeth*. Cambridge University Press.

Hobson, K. A. (1999). Tracing origins and migration of wildlife using stable isotopes: A review. *Oecologia*, 120(3), 314–326. https://doi.org/10.1007/s004420050865

Holt, E., Evans, J. A., & Madgwick, R. (2021). Strontium ($^{87}Sr/^{86}Sr$) mapping: A critical review of methods and approaches. *Earth-Science Reviews*, 216, 103593. https://www.sciencedirect.com/science/article/pii/S0012825221000933

Ingram, B. L., & Weber, P. K. (1999). Salmon origin in California's Sacramento–San Joaquin river system as determined by otolith strontium isotopic composition. *Geology*, 27(9), 851–854. https://doi.org/10.1130/0091-7613(1999)027<0851:SOICSS>2.3.CO;2

Koch, P. L., Fisher, D. C., & Dettman, D. (1989). Oxygen isotope variation in the tusks of extinct proboscideans: A measure of season of death and seasonality. *Geology*, 17(6), 515–519. https://doi.org/10.1130/0091-7613(1989)017<0515:OIVITT>2.3.CO;2

Kowalik, N., Anczkiewicz, R., Müller, W., Spötl, C., Bondioli, L., Nava, A., Wojtal, P., Wilczyński, J., Koziarska, M., & Matyszczak, M. (2023). Revealing seasonal woolly mammoth migration with spatially-resolved trace element, Sr and O isotopic records of molar enamel. *Quaternary Science Reviews*, 306, 108036. https://www.sciencedirect.com/science/article/pii/S0277379123000847

Larramendi, A. (2015). Shoulder height, body mass, and shape of proboscideans. *Acta Palaeontologica Polonica*, 61(3), 537–574. https://doi.org/10.4202/app.00136.2014

Lazzerini, N., Balter, V., Coulon, A., Tacail, T., Marchina, C., Lemoine, M., Bayarkhuu, N., Turbat, T., Lepetz, S., & Zazzo, A. (2021). Monthly mobility inferred from isoscapes and laser ablation strontium isotope ratios in caprine tooth enamel. *Scientific Reports*, 11(1), 2277. https://doi.org/10.1038/s41598-021-81923-z

Lewis, J., Pike, A. W. G., Coath, C. D., & Evershed, R. P. (2017). Strontium concentration, radiogenic ($^{87}Sr/^{86}Sr$) and stable ($\delta^{88}Sr$) strontium isotope systematics in a controlled feeding study. *STAR: Science & Technology of Archaeological Research*, 3(1), 45–57. https://doi.org/10.1080/20548923.2017.1303124

Ma, C., Vander Zanden, H. B., Wunder, M. B., & Bowen, G. J. (2020). assignR: An r package for isotope-based geographic assignment. *Methods in Ecology and Evolution*, 11(8), 996–1001. https://doi.org/10.1111/2041-210X.13426

Magozzi, S., Vander Zanden, H. B., Wunder, M. B., & Bowen, G. J. (2019). Mechanistic model predicts tissue–environment relationships and trophic shifts in animal hydrogen and oxygen isotope ratios. *Oecologia*, 191(4), 777–789. https://doi.org/10.1007/s00442-019-04532-8

Makarewicz, C. A., & Sealy, J. (2015). Dietary reconstruction, mobility, and the analysis of ancient skeletal tissues: Expanding the prospects of stable isotope research in archaeology. *Journal of Archaeological Science*, 56, 146–158. https://www.sciencedirect.com/science/article/pii/S0305440315000813

Makowski, D., Ben-Shachar, M. S., & Lüdecke, D. (2019). bayestestR: Describing effects and their uncertainty, existence and significance within the Bayesian framework. *Journal of Open Source Software*, 4(40), 1541. https://doi.org/10.21105/joss.01541

Martínez del Rio, C., & Carleton, S. A. (2012). How fast and how faithful: The dynamics of isotopic incorporation into animal tissues. *Journal of Mammalogy*, 93(2), 353–359. https://doi.org/10.1644/11-MAMM-S-165.1

Martínez del Rio, C., Wolf, N., Carleton, S. A., & Gannes, L. Z. (2009). Isotopic ecology ten years after a call for more laboratory experiments. *Biological Reviews*, 84(1), 91–111. https://doi.org/10.1111/j.1469-185X.2008.00064.x

McElreath, R. (2018). *Statistical rethinking: A Bayesian course with examples in R and Stan*. Chapman and Hall/CRC.

Meiggs, D. C. (2007). Visualizing the seasonal round: A theoretical experiment with strontium isotope profiles in ovicaprine teeth. *Anthropozoologica*, 42(2), 107–127. https://sciencepress.mnhn.fr/en/periodiques/anthropozoologica/42/2/visualiser-la-mobilite-saisonniere-un-modele-theorique-partir-des-profils-isotopiques-du-strontium-dans-les-dents-de-caprines

Miller, J. H., Fisher, D. C., Crowley, B. E., Secord, R., & Konomi, B. A. (2022). Male mastodon landscape use changed with maturation (late Pleistocene, North America). *Proceedings of the National Academy of Sciences of the United States of America*, 119(25), e2118329119. https://doi.org/10.1073/pnas.2118329119

Passey, B. H., & Cerling, T. E. (2002). Tooth enamel mineralization in ungulates: Implications for recovering a primary isotopic time-series. *Geochimica et Cosmochimica Acta*, 66(18), 3225–3234. https://doi.org/10.1016/S0016-7037(02)00933-X

Phillips, D. L., & Eldridge, P. M. (2006). Estimating the timing of diet shifts using stable isotopes. *Oecologia*, 147(2), 195–203. https://doi.org/10.1007/s00442-005-0292-0

Phillips, D. L., & Koch, P. L. (2002). Incorporating concentration dependence in stable isotope mixing models. *Oecologia*, 130(1), 114–125. https://doi.org/10.1007/s004420100786

Plummer, M. (2021). *rjags: Bayesian graphical models using MCMC*. R package. https://cran.r-project.org/web/packages/rjags/index.html

R Core Team. (2023). *R: A language and environment for statistical computing*. R Foundation for Statistical Computing. https://www.R-project.org/

Sakamoto, T., Komatsu, K., Shirai, K., Higuchi, T., Ishimura, T., Setou, T., Kamimura, Y., Watanabe, C., & Kawabata, A. (2019). Combining microvolume isotope analysis and numerical simulation to reproduce fish migration history. *Methods in Ecology and Evolution*, 10(1), 59–69. https://doi.org/10.1111/2041-210X.13098

Smith, C. E. (1998). Cellular and chemical events during enamel maturation. *Critical Reviews in Oral Biology & Medicine*, 9(2), 128–161. https://doi.org/10.1177/10454411980090020101

Suga, S. (1982). Progressive mineralization pattern of developing enamel during the maturation stage. *Journal of Dental Research*, 61, 1532–1542.

Thomas, S. M., & Crowther, T. W. (2015). Predicting rates of isotopic turnover across the animal kingdom: A synthesis of existing data. *Journal of Animal Ecology*, 84(3), 861–870. https://doi.org/10.1111/1365-2656.12326

Tieszen, L. L., Boutton, T. W., Tesdahl, K. G., & Slade, N. A. (1983). Fractionation and turnover of stable carbon isotopes in animal tissues: Implications for $\delta^{13}C$ analysis of diet. *Oecologia*, 57(1), 32–37. https://doi.org/10.1007/BF00379558

Trueman, C. N., & St John Glew, K. (2019). Chapter 6—Isotopic tracking of marine animal movement. In K. A. Hobson & L. I. Wassenaar (Eds.), *Tracking animal migration with stable isotopes* (2nd ed., pp. 137–172). Academic Press. https://www.sciencedirect.com/science/article/pii/B9780128147238000064

Uno, K. T., Fisher, D. C., Schuster, G., Wittemyer, G., Douglas-Hamilton, I., Omondi, P., Litoroh, M., & Cerling, T. E. (2020). High-resolution

stable isotope profiles of modern elephant (*Loxodonta africana*) tusk dentin and tail hair from Kenya: Implications for identifying seasonal variability in climate, ecology, and diet in ancient proboscideans. *Palaeogeography, Palaeoclimatology, Palaeoecology, 559*, 109962. https://www.sciencedirect.com/science/article/pii/S0031018220304077

Uno, K. T., Fisher, D. C., Wittemyer, G., Douglas-Hamilton, I., Carpenter, N., Omondi, P., & Cerling, T. E. (2020). Forward and inverse methods for extracting climate and diet information from stable isotope profiles in proboscidean molars. *Quaternary International, 557*, 92–109. http://www.sciencedirect.com/science/article/pii/S1040618220303426

Vander Zanden, M. J., Clayton, M. K., Moody, E. K., Solomon, C. T., & Weidel, B. C. (2015). Stable isotope turnover and half-life in animal tissues: A literature synthesis. *PLoS ONE, 10*(1), e0116182. https://doi.org/10.1371/journal.pone.0116182

Weber, M., Tacail, T., Lugli, F., Clauss, M., Weber, K., Leichliter, J., Winkler, D. E., Mertz-Kraus, R., & Tütken, T. (2020). Strontium uptake and intra-population $^{87}Sr/^{86}Sr$ variability of bones and teeth—Controlled feeding experiments with rodents (*Rattus norvegicus, Cavia porcellus*). *Frontiers in Ecology and Evolution, 8*(434). https://doi.org/10.3389/fevo.2020.569940

Willmes, M., Glessner, J. J. G., Carleton, S. A., Gerrity, P. C., & Hobbs, J. A. (2016). $^{87}Sr/^{86}Sr$ isotope ratio analysis by laser ablation MC-ICP-MS in scales, spines, and fin rays as a nonlethal alternative to otoliths for reconstructing fish life history. *Canadian Journal of Fisheries and Aquatic Sciences, 73*(12), 1852–1860. https://doi.org/10.1139/cjfas-2016-0103

Wolf, N., Carleton, S. A., & Martínez del Rio, C. (2009). Ten years of experimental animal isotopic ecology. *Functional Ecology, 23*(1), 17–26. https://doi.org/10.1111/j.1365-2435.2009.01529.x

Wooller, M. J., Bataille, C., Druckenmiller, P., Erickson, G. M., Groves, P., Haubenstock, N., Howe, T., Irrgeher, J., Mann, D., Moon, K., Potter, B. A., Prohaska, T., Rasic, J., Reuther, J., Shapiro, B., Spaleta, K. J., & Willis, A. D. (2021). Lifetime mobility of an Arctic woolly mammoth. *Science, 373*(6556), 806–808. https://doi.org/10.1126/science.abg1134

Wunder, M. B. (2010). Using isoscapes to model probability surfaces for determining geographic origins. In J. B. West, G. J. Bowen, T. E. Dawson, & K. P. Tu (Eds.), *Isoscapes: Understanding movement, pattern, and process on earth through isotope mapping* (pp. 251–270). Springer Netherlands. https://doi.org/10.1007/978-90-481-3354-3_12

Wunder, M. B. (2012). Determining geographic patterns of migration and dispersal using stable isotopes in keratins. *Journal of Mammalogy, 93*(2), 360–367. https://doi.org/10.1644/11-MAMM-S-182.1

Yang, D. (2023). BITS: Bayesian isotope turnover and sampling model. *Zenodo*, https://doi.org/10.5281/zenodo.7741883

SUPPORTING INFORMATION

Additional supporting information can be found online in the Supporting Information section at the end of this article.

Data S1: Supplementary text, tables, figures, and references.

How to cite this article: Yang, D., Bowen, G. J., Uno, K. T., Podkovyroff, K., Carpenter, N. A., Fernandez, D. P., & Cerling, T. E. (2023). BITS: A Bayesian Isotope Turnover and Sampling model for strontium isotopes in proboscideans and its potential utility in movement ecology. *Methods in Ecology and Evolution, 00*, 1–14. https://doi.org/10.1111/2041-210X.14218